Pyrogenic HONO seen from space: insights from global IASI observations.

https://doi.org/10.5194/egusphere-2023-2707

Response to Referee #1

The paper by Franco et al. presents pyrogenic nitrous acid (HONO) detection and total column quantification based on satellite observations from IASI on Metop since 2007. The detection method is based on the hyperspectral range index to identify spectra with observable HONO signature. Two spectral regions are investigated (820-890 cm-1 and 1210-1305 cm-1) to detect HONO in fire plumes and it is shown the 1210-1305 cm-1 band is the most sensitive because less affected by interfering species. An additional filter combining the HONO detection with ammonia (NH3) and ethylene (C2H4) detection, also emitted by fires, is proposed to limit false detections of pyrogenic HONO in IASI spectra. The paper provides an analysis of the pyrogenic HONO detections in terms of spatial and temporal distributions from the entire archive of IASI A, B, and C instruments and compares the results with the TROPOMI HONO product available at the end of the period and to MODIS fire products. The IASI HONO detection is the most reliable for the mid and high latitudes of both hemispheres. The reasons of the low detection rate in the tropics are discussed. The paper highlights the increase of pyrogenic HONO detection during the last five years in agreement with the increase of wildfire activities. Finally, the paper proposes an estimation of HONO total columns using an artificial neural network architecture, already applied to other low-absorbing species retrieved from IASI. A tentative of comparison with TROPOMI HONO columns estimation is provided for two case studies, and the limitations of such comparisons are discussed.

The paper provides an important step forward in satellite remote sensing of wildfire impacts on atmospheric composition, focusing on a challenging species, HONO. Nitrous acid is a key atmospheric species as a major source of hydroxyl radical, but important gaps remain in our knowledge of its global budget due to the difficulties to measure it at large scales. The new HONO IASI product presented in the paper complements the recent TROPOMI HONO product, especially with nighttime observations to probe globally HONO in pyrogenic plumes, and the long time series available is of great value to improve knowledge on HONO atmospheric budget. The paper is well structured, written and documented. The results are well argued, and limitations of the HONO product mostly discussed. The paper is suitable for publication in ACP after some clarifications.

We would like to thank the Referee for the positive evaluation of this paper and for the comments that contributed to improving the manuscript. Please find in blue here below our response to the comments and the changes made to the manuscript. Furthermore, we have revised several figures to improve both their clarity and consistency across the entire manuscript.

Main comments:

My main comments concern the description of the detection and retrieval approaches, which needs some clarifications. These approaches have been already described in other papers for other species and the authors referred to these papers, but some details are missing to understand the specificities to HONO detection and retrieval.

Concerning the detection method (section 2.1), it is not clear which assumptions are made on the atmospheric concentrations of HONO and interfering species to calculate the Jacobian K. We understand later in the text (line 376) that the US 1976 standard atmosphere is used as well as a HONO profile including a narrow layer (line 375) but without much more details. Is the HONO profile considered as a gaussian profile, as described in section 4? What is the impact of the shape and the height of the HONO peak on the detection based on the HRI? These details should be provided earlier in the text (section 2.1) and completed. The authors should also specify how they calculate the generalized covariance matrix Sy. Is this matrix diagonal, for example?

The HONO detection with the HRI is not significantly influenced by the assumed profile and abundance of HONO or the atmospheric conditions that were used to construct the Jacobian. This is illustrated in the figure below, which displays, in blue, the Jacobian used in this study, which has been generated based on a HONO total column of 1.77 x 10^{17} molec cm^{-2} confined to a narrow layer (~1 km thick) at 2 km altitude, assuming the US 1976 standard atmosphere. The second Jacobian, in red, has been generated assuming a HONO total column more than one order of magnitude lower (7.03 x 10^{15} molec cm^{-2}), confined in a half-thickness layer at 4 km altitude, for a mid-latitude atmosphere in summertime. The figure below shows that all these changes do not significantly affect the intensity of the Jacobian, nor does it change its shape.

Please note that Lines 375-376 do not refer to the Jacobian that is used to calculate the HRI, but instead to different Jacobians that are generated specifically for calculating the IASI's detection threshold of HONO for various altitudes through Eq. 6. In this specific case, a Gaussian profile was assumed, peaking at various altitudes between 0 and 14 km, and with a standard deviation (σ) of 300 m representing a narrow atmospheric layer.

We have detailed the calculation of the covariance matrix as follows:

"*This set of background spectra, and the associated S_y and $\bar{y}$, are determined via an iterative filtering process (Franco et al., 2018; Clarisse et al., 2019). Beginning with a comprehensive set of IASI spectra, this process consists, at each step, in calculating S_y and $\bar{y}$ associated with the given spectra, determining the HRI for each observation, discarding all spectra with detectable target gas signatures from the set, and calculating the factor N.*"

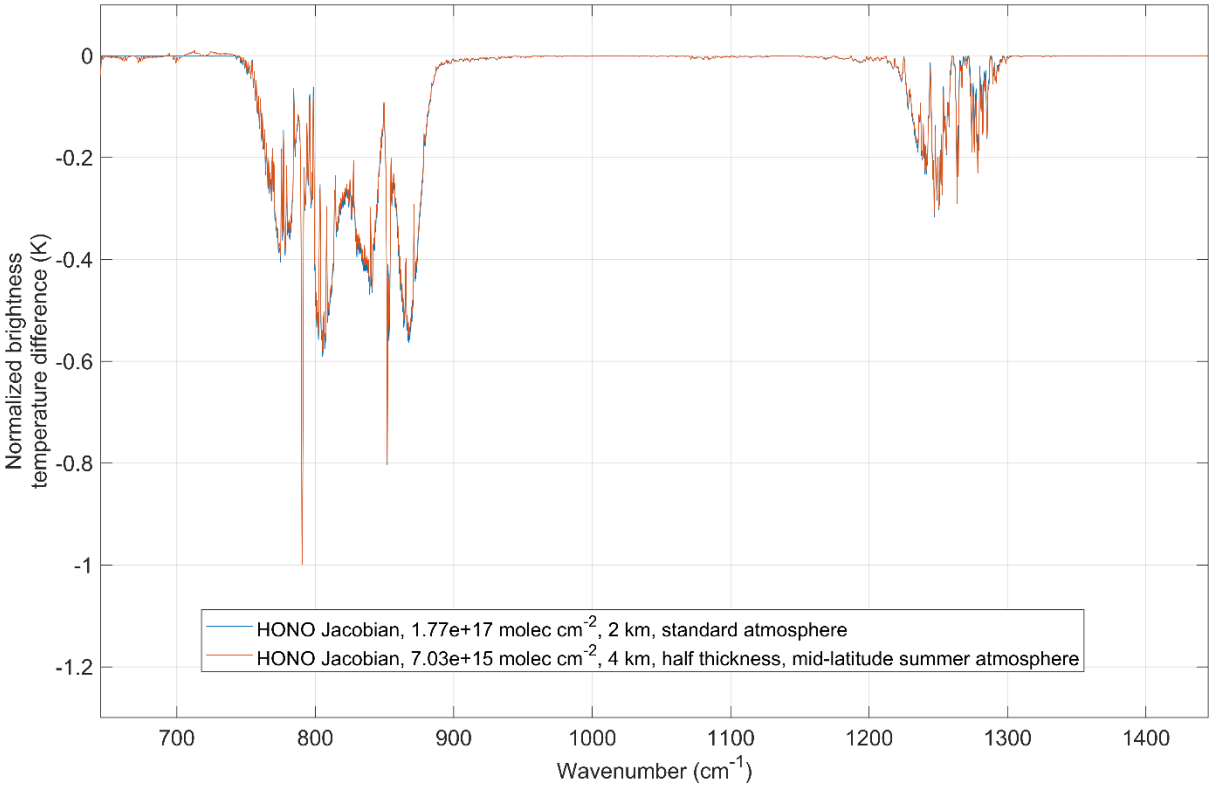

Similarly, the set-up for the retrieval of HONO in section 4.1 is confused. It is not clear for me what are the inputs and the outputs of the NN. Indeed, it is not described how the parameters related to the abundance and vertical distribution are chosen to feed the NN and if they are retrieved at the output of the NN or if it is just the total columns. Line 517 it seems these parameters are variable from one pixel to another in the inputs (on which basis/assumption these variations are chosen? Is a model used?) but line 523, it seems that σ is fixed to 350m for all the pixels without any discussion of this choice, whereas a range of possible variations from 100m to 3km is mentioned in Eq 8. This should be clarified.

We now better explain in Sect 4.1 what the inputs and outputs of the NN for the HONO retrieval are, and we clarify how the parameters z_0 and σ are defined:

"The first step of the ANNI retrieval procedure consists in calculating an HRI for each observed spectrum, as described earlier (Sect. 2.1). In the second step, each HRI is converted into a single pixel estimate $\hat{X}^a$ of the gas total column via a scaling factor SF^a (the superscript a indicates the use of an assumed vertical distribution of the target gas):

$$\hat{X}^a = {HRI}/{SF^a} \qquad (7)$$

In ANNI, SF^a is estimated by an artificial feedforward neural network (NN) that considers the state of the Earth's atmosphere and surface. For a given IASI observation, the NN input parameters include the HONO HRI itself, the temperature (15 levels) and the H_2O (7 levels) profiles, surface temperature, pressure, emissivity, and the IASI viewing angle associated this observation. In addition, two parameters z_0 and σ are provided to the NN to characterize the HONO vertical profile following a Gaussian distribution:

$$vmr_{HONO} = k \times exp\left(\frac{-(z-z_0)^2}{2\sigma^2}\right) \qquad (8)$$

with k a multiplicative factor, z_0 ranging from the surface up to 20 km altitude, and σ comprised between 100 m and 3 km. This vertical profile parametrization, which is the same as used for the NH_3 and C_2H_4 IASI products, allows to approximate a wide variety of profiles (Whitburn et al., 2016; Van Damme et al., 2021; Franco et al., 2022). In particular, for HONO, this profile can be used to model fire plumes of various thicknesses and located at various altitudes from the surface to the lower stratosphere.

The NN consists of two computational layers of 12 nodes. It is trained based on an extensive set of synthetic spectra (>500,000 spectra) generated with representative input data of the atmospheric and surface conditions as well as parameters related to the abundance and vertical distribution of HONO (σ, z_0, and k). For each IASI observation, the NN estimates SF^a based on the input parameters and provides the $HRI/\hat{X}^a$ ratio as the main output (along with other ancillary outputs; see Sect. 4.2), which is subsequently converted to $\hat{X}^a$. The primary advantage of using this ratio as output instead of $\hat{X}^a$ itself is to ensure that the retrieval on noisy HRI does not result in a biased product (see Whitburn et al., 2016, for more on the rationale behind this ratio).

For the ANNI retrieval, the meteorological input variables are sourced from the European Center for Medium-Range Weather Forecasts (ECMWF) ERA5 reanalysis (Hersbach et al., 2020). This choice ensures a more comprehensive and coherent dataset across the entire IASI operational time series than with the IASI Level 2 data (Van Damme et al., 2021).

Ideally, z_0 and σ should be tailored for each singe-pixel HONO retrieval based on the actual altitude and thickness of the fire plume. Unfortunately, such third-party information is rarely available. Consequently, for the standard ANNI v4 HONO product, the parameter z_0 is set based on a 1° × 1° monthly climatology of fire plume altitudes derived from CALIPSO data (Sect. 3.2), and a value of 350 m is assigned for σ. The same approach was applied to estimate the dust altitude for retrieving dust optical depths from IASI observations (Clarisse et al., 2019). However, since the NN has been trained to encompass a broad range of z_0 and σ values, these parameters can be adjusted for an optimized HONO retrieval if information on the altitude and thickness of a specific fire plume under study becomes available."

Specific comments:

Line 113: the authors could specify that the spectra in brightness temperature are considered for the HRI calculation.

The spectra are considered in radiance for the HRI calculation. However, in the manuscript, such as in Fig. 2, the IASI spectra shown as examples are displayed in brightness temperature as this unit is more convenient for display purposes.

Lines 170-171: trace gases and surface emissivity are mentioned but what about aerosol spectral signatures? Do they interfere with HONO signature?

In Clarisse et al. (2010, 2013), it has been shown that smoke aerosols in the thermal infrared are typically characterized by weak and broad spectral signatures spanning several hundred cm^{-1}, thus primarily affecting the spectral baseline. The effect of such aerosols on the IASI spectra is marginal because of the size of these particles. As a result, even for huge fires, IASI retrievals remain mostly insensitive to smoke aerosols. For instance, it can be seen in Fig. 2a and Fig. A3a (for fires in Canada and Portugal, respectively) that the baseline of the IASI spectra is not affected. So far, smoke aerosols have only been clearly identified in IASI spectra during the exceptional Australian fires. This is

illustrated in the new Fig. A2a (see our response to the next comment) by the noticeable change in the baseline of the IASI spectrum compared to the examples in Fig. 2a and Fig. A3a.

Lines 210-213: as up to now, detection of HONO with IASI was done only in Australian fires, it would have been interesting to provide an example of the magnitude of the HONO spectral contributions also in an Australian fire case to see how higher it is compared to other fires.

The figure below reproduces Figs 2 and A2, showcasing an IASI/Metop-A spectrum captured in a fresh fire plume during the 2019/2020 Australian wildfires. The spectral analysis aligns with previous conclusions drawn for other fire plumes presented in the manuscript, but the HONO HRI values here are notably elevated, reaching 36.04 and 56.62 in the first and second absorption bands, respectively. This underscores the exceptional intensity of this fire event. We have added this new figure to the Appendix and referred to it in Section 2.3 as follows:

"*For comparison, the spectral analysis of an IASI observation in a fresh Australian fire plume from December 2019 (depicted in Fig. A2) indicates markedly higher HONO HRI enhancements, with values of 36.04 for the 820-890 cm^{-1} range and 56.62 for the 1210-1305 cm^{-1} window.*"

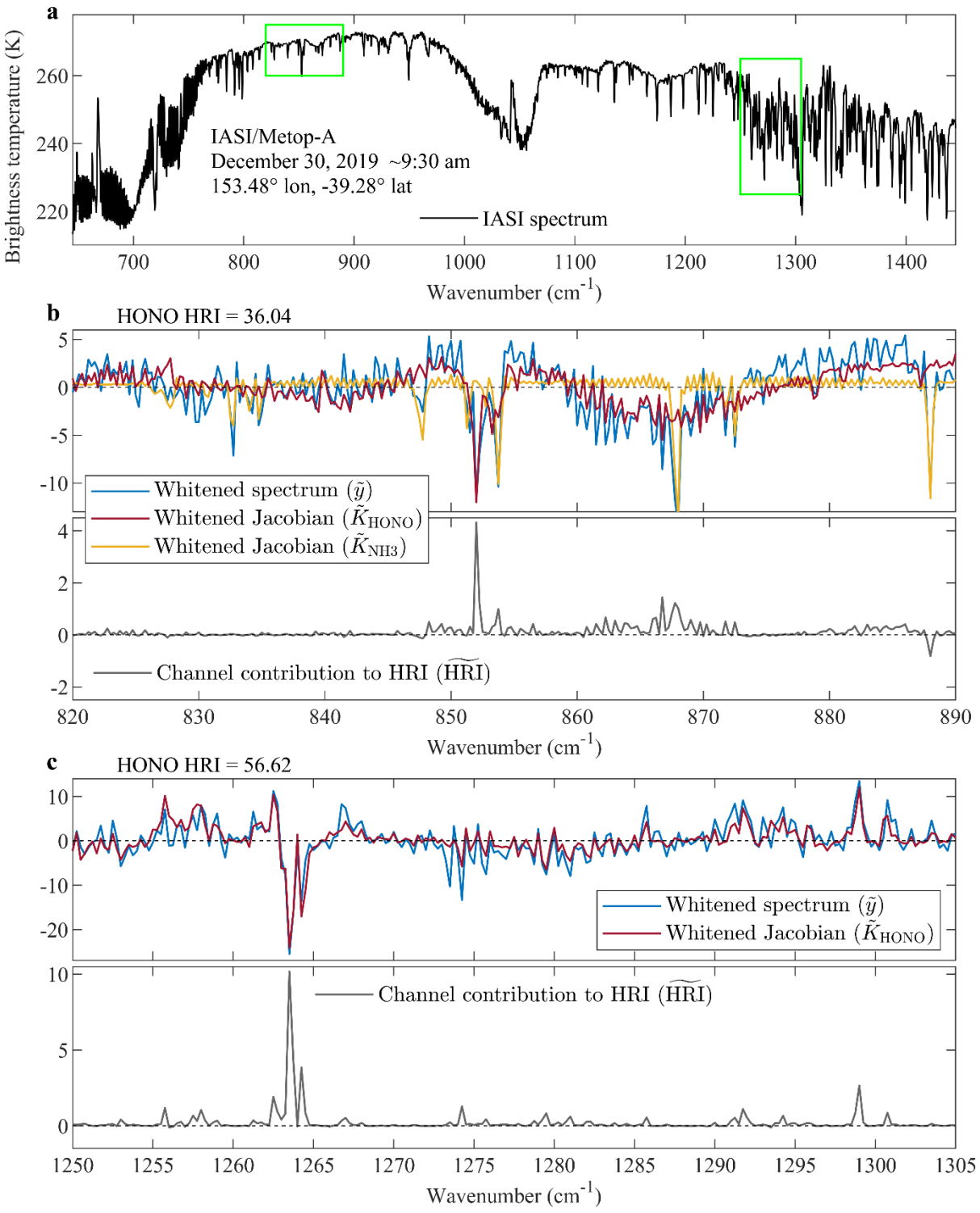

Section 2.4: The authors have demonstrated that the 820-890 cm-1 region is less sensitive to HONO detection compared to the 1210-1305 cm-1 region. What is the interest to provide the filter for this spectral region, which is not leveraged after? What would be the interest to use both regions for detection and retrievals?

We thank the Referee for this comment. Throughout Sect. 2, we conducted various exercises to evaluate both spectral ranges, including a comparison of HRI intensity in fresh fire plumes (Sect. 2.2),

a thorough spectral analysis with the whitening (Sect. 2.3), and a comparison of the specific detection filters set up for each absorption band (Sect. 2.4). While we concluded Sect. 2.4 by specifying our focus on the 1210-1305 cm^{-1} HRI for the rest of the study, we deliberately included some results from the 820-890 cm^{-1} range in our analysis in Sect. 3 (and related figures in appendix) as it allows us to perform comparisons between the two HONO bands. The consistency observed in our results across these two ranges provides indeed valuable cross-verification, bolstering the robustness of our findings. We are convinced that this approach is important for establishing the reliability of our methodology and results, and that it enhances the overall strength and credibility of our study. Please note, however, that the 820-890 cm^{-1} band is not used for the retrievals in Sect. 4.

To clarify our approach, we have added the following statements, respectively, in Sect. 2.1 and at the end of Sect. 2.4:

Line 132: "*Throughout Sect. 2, we systematically assess the advantages and limitations of each spectral range for the detection of pyrogenic HONO.*"

Line 278: "*Considering the advantages presented in Sect. 2 by the 1210-1305 cm^{-1} band for the detection of pyrogenic HONO with IASI, we will focus on the HRI calculated within this range from Sect. 3 onwards. Nonetheless, results obtained with the 820-890 cm^{-1} band will also be briefly presented, as they allow for important cross-verification.*"

Figure 5: IASI and TROPOMI are not compared for the same period (IASI since 2007, TROPOMI since 2018). Are the results different if the same period is used for the comparison?

Please find below a revised version of Fig. 5, using only the IASI data since 2018. It exhibits only marginal differences from the original Fig. 5, based on the entire IASI time series, and does not alter any conclusions of the analysis. For consistency, only the MODIS data since 2018 are displayed. We are now using this revised version of Fig. 5 in the manuscript.

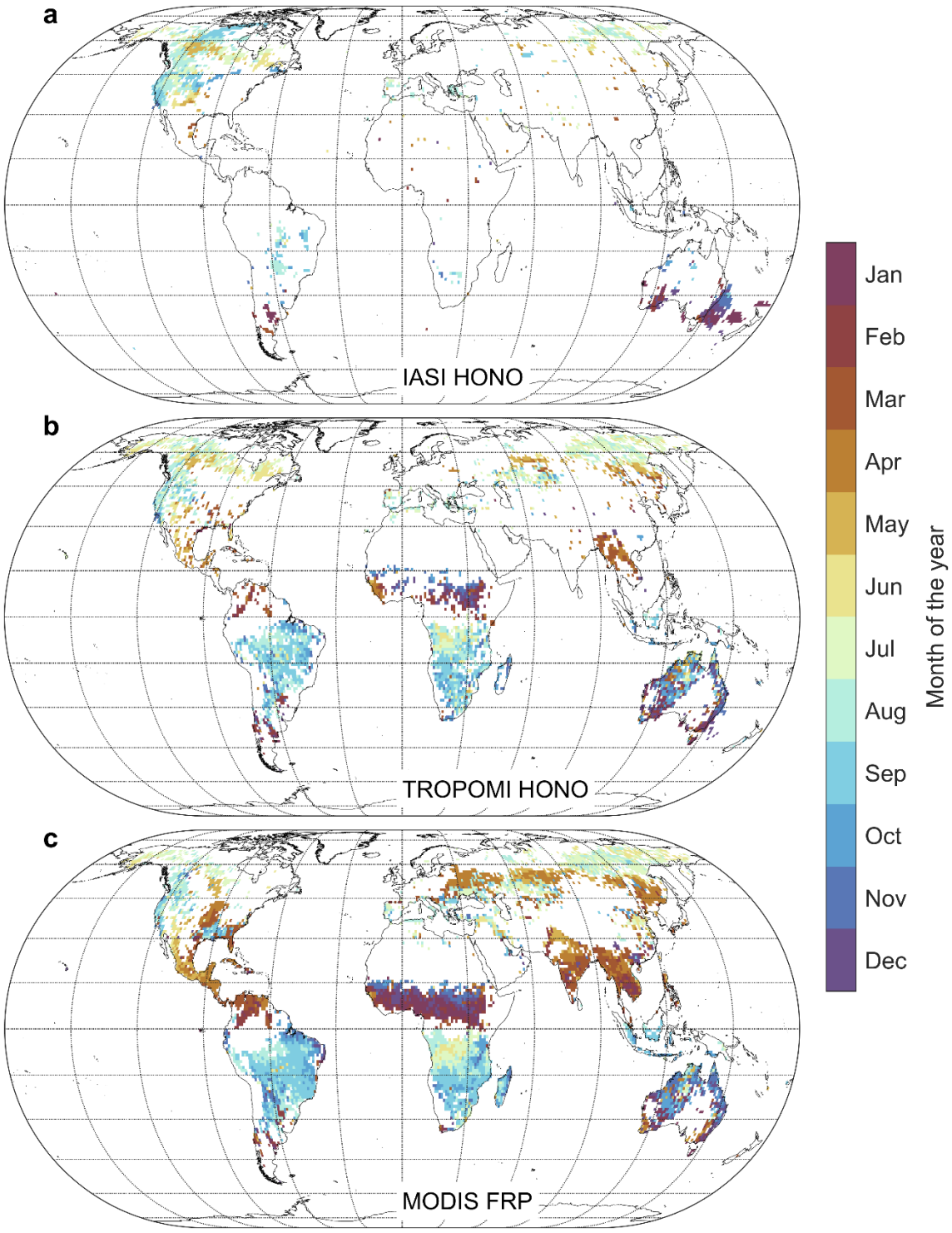

Line 375: the authors should specify what they mean by narrow layer (see main comments).

This is now specified in the manuscript as follows:

"With S_y the generalized covariance matrix of IASI used in the calculation of the HRI (see Sect. 2.1), and K_z the spectral Jacobian with respect to HONO distributed vertically following a Gaussian profile peaking at the altitude z (for z values ranging between 0 and 14 km altitude) and with a standard deviation (σ) of 300 m around z, representing a narrow atmospheric layer."

Line 445 and around when the authors discuss the difference between the early time series and the more recent ones: at the beginning of IASI-A lifetime, only one pixel out of two was distributed. In the time series presented here, is it still the case or all the pixels are considered? If not, this may impact the number of detections for this period.

In the early IASI time series, all Level-1 data were distributed, but Level-2 data (temperature, water vapour, etc.) were indeed only available for one pixel out of two. However, for the IASI HONO product and the other ANNI v4 products (e.g., NH_3 and C_2H_4), we use ECMWF ERA5 reanalysis data (Hersbach et al., 2020) instead of IASI Level-2 data throughout the IASI time series. Moreover, we use our own cloud product, derived directly from IASI radiances (Whitburn et al., 2022). This allows us to exploit consistently all the observations from the IASI time series for both HRI detection and retrieval of HONO.

Line 477-492: It is not clear for me to what conclusion for HONO the analysis of ethylene leads.

We agree with the Referee that we did not motivate enough the analysis of C_2H_4 in Sect. 3.2. This is now done as follows:

"*To rule out potential other reasons for the observed am/pm difference, it is useful to look at another short-lived biomass burning tracer, namely C_2H_4. In Fig. 12, we compare […]*

[…] Although reactions with OH and O_3 are expected to proceed more slowly during nighttime hours due to lower temperatures, we do not observe a prevalence of C_2H_4 detections with the evening IASI measurements, such as observed for HONO (Fig. 12). This suggests, first, that variations in photochemistry between daytime and nighttime do not significantly impact C_2H_4 concentrations in fire plumes. Second, it implies that the presence of measurement artefacts responsible for large am/pm differences in HONO detection can be ruled out, confirming that the absence of photolysis is the primary driver of the more numerous HONO detections at nighttime."

Line 518: What do the authors mean by "actual retrieval"? Is it the retrieval based on a radiative transfer model, or is it the ANNI retrieval?

We meant "*the ANNI retrieval*". This has been corrected.

Section 4.3, discussion of the Woosley Fire: the authors elaborate on the time evolution and the spatial extension of the plumes using IASI and TROPOMI observations. I would be more cautious about what we can draw from these comparisons, given the assumptions and the large uncertainties in the observations and the differences in terms of sensitivity of the two instruments.

We agree with the Referee that the discussions in Sect. 4.3 are not straightforward given the uncertainties and instrumental differences. This is why, in the second paragraph of Sect. 4.3, we alert the reader: "*The goal here is not to perform a quantitative cross-validation of the two satellite products. Comparing at face value the IASI and TROPOMI VCDs of HONO is indeed particularly challenging given the intrinsic differences between the two satellite sounders. The main ones are: […] For these reasons, the primary objective is to showcase the ANNI v4 HONO product and to provide a qualitative assessment of the HONO VCDs from IASI and TROPOMI.*"

In addition, we further discuss the IASI/TROPOMI disparities and their impact on HONO measurements in Sect. 4.4. Notably, we write at the beginning of Sect. 4.4: "*Despite improvements, the retrieval of HONO VCDs in fire plumes from both IASI and TROPOMI remains challenging and currently requires assumptions that introduce uncertainties on the retrieved quantities and hinder a more accurate comparison between their respective HONO products.*"

We reiterate these caveats in the conclusion: "*The HONO columns from these two sounders show promising results with retrieved VCDs in the same order of magnitude. Nonetheless, this comparison cannot serve as cross-validation of the satellite products, given the distinct characteristics and overpass times of the two sounders.*"

Technical corrections:

Figures quality when printed is low.

We thank the Referee for bringing this point to our attention. We created the manuscript's PDF with LaTeX, utilizing figures saved in a vectorized format. Upon examination, the figures appear satisfactory even when zoomed in on screen. We commit to ensuring the use of figures with the highest quality in the next steps.

Figure 3: the colorbars should be reversed. C2H4 colorbars is below NH3 plots and vice versa.

The colorbars in Fig. 3 are correct. The x-axis of the panels in the left column indicates the NH_3 HRI of the observations displayed in the scatter plots, and these observations are colour-coded based on their C_2H_4 HRI (colorbar). The panels in the right column depict the same relationships, but with the C_2H_4 HRI on the x-axis and the NH_3 HRI as the colour code. We have also slightly modified this figure to enhance its clarity.

Line 481: change "The IASI retrieval" to "The IASI detection".

Done. Thank you for spotting this mistake.

References

- Clarisse, L., Hurtmans, D., Prata, A. J., Karagulian, F., Clerbaux, C., De Mazière, M., and Coheur, P.-F.: Retrieving radius, concentration, optical depth, and mass of different types of aerosols from high-resolution infrared nadir spectra, Applied Optics, 49, 3713, https://doi.org/10.1364/ao.49.003713, 2010.
- Clarisse, L., Coheur, P.-F., Prata, F., Hadji-Lazaro, J., Hurtmans, D., and Clerbaux, C.: A unified approach to infrared aerosol remote sensing and type specification, Atmospheric Chemistry and Physics, 13, 2195–2221, https://doi.org/10.5194/acp-13-2195-2013, 2013.
- Clarisse, L., Clerbaux, C., Franco, B., Hadji-Lazaro, J., Whitburn, S., Kopp, A. K., Hurtmans, D., and Coheur, P.-F.: A Decadal Data Set of Global Atmospheric Dust Retrieved From IASI Satellite Measurements, Journal of Geophysical Research: Atmospheres, 124, 1618–1647, https://doi.org/10.1029/2018jd029701, 2019.
- Franco, B., Clarisse, L., Van Damme, M., Hadji-Lazaro, J., Clerbaux, C., and Coheur, P.-F.: Ethylene industrial emitters seen from space, Nature Communications, 13, 6452, https://doi.org/10.1038/s41467-022-34098-8, 2022.
- Hersbach, H., Bell, B., Berrisford, P., Hirahara, S., Horányi, A., Munoz-Sabater, J., Nicolas, J., Peubey, C., Radu, R., Schepers, D., Simmons, A., Soci, C., Abdalla, S., Abellan, X., Balsamo, G., Bechtold, P., Biavati, G., Bidlot, J., Bonavita, M., Chiara, G., Dahlgren, P., Dee, D., Diamantakis, M., Dragani, R., Flemming, J., Forbes, R., Fuentes, M., Geer, A., Haimberger, L., Healy, S., Hogan, R. J., Hólm, E., Janisková, M., Keeley, S., Laloyaux, P., Lopez, P., Lupu, C., Radnoti, G., Rosnay, P., Rozum, I., Vamborg, F., Villaume, S., and Thépaut, J.-N.: The ERA5 global reanalysis, Quarterly

Journal of the Royal Meteorological Society, 146, 1999–2049, https://doi.org/10.1002/qj.3803, 2020.

- Van Damme, M., Clarisse, L., Franco, B., Sutton, M. A., Erisman, J. W., Kruit, R. W., van Zanten, M., Whitburn, S., Hadji-Lazaro, J., Hurtmans, D., Clerbaux, C., and Coheur, P.-F.: Global, regional and national trends of atmospheric ammonia derived from a decadal (2008-2018) satellite record, Environmental Research Letters, 16, 055 017, https://doi.org/10.1088/1748-9326/abd5e0, 2021.
- Whitburn, S., Van Damme, M., Clarisse, L., Bauduin, S., Heald, C. L., Hadji-Lazaro, J., Hurtmans, D., Zondlo, M. A., Clerbaux, C., and Coheur, P.-F.: A flexible and robust neural network IASI-NH3 retrieval algorithm, Journal of Geophysical Research: Atmospheres, 121, 6581–6599, https://doi.org/10.1002/2016jd024828, 2016.
- Whitburn, S., Clarisse, L., Crapeau, M., August, T., Hultberg, T., Coheur, P. F., and Clerbaux, C.: A CO2-independent cloud mask from Infrared Atmospheric Sounding Interferometer (IASI) radiances for climate applications, Atmospheric Measurement Techniques, 15, 6653–6668, https://doi.org/10.5194/amt-15-6653-2022, 2022.